PEROVSKITES

Synthesis of $LaWN_3$ nitride perovskite with polar symmetry

Kevin R. Talley[1,2], Craig L. Perkins[1], David R. Diercks[2], Geoff L. Brennecka[2]*, Andriy Zakutayev[1]*

Oxide materials with the perovskite structure have been used in sensors and actuators for half a century, and halide perovskites transformed photovoltaics research in the past decade. Nitride perovskites have been computationally predicted to be stable, but few have been synthesized, and their properties remain largely unknown. We synthesized and characterized a nitride perovskite lanthanum tungsten nitride ($LaWN_3$) in the form of oxygen-free sputtered thin films, according to spectroscopy, scattering, and microscopy techniques. We report a large piezoelectric response measured with scanning probe microscopy that together with synchrotron diffraction confirm polar symmetry of the perovskite $LaWN_3$. Our $LaWN_3$ synthesis should inspire growth of other predicted nitride perovskites, and measurements of their properties could lead to functional integration with nitride semiconductors for microelectromechanical devices.

Nitride materials are revolutionizing the way humans access information and communicate with others. For example, 4th-generation (4G) wireless networks feature piezoelectric aluminum nitride (AlN) film bulk acoustics resonators (FBARs). Radio-frequency (RF) transistors based on semiconducting gallium nitride (GaN) are becoming an important part of the 5G telecommunication technology. The emerging telecommunication infrastructure would further benefit from improved piezoelectric materials, especially if they are easy to integrate with nitride semiconductors. We synthesized lanthanum tungsten nitride ($LaWN_3$) thin films with a perovskite crystal structure, polar symmetry, and strong piezoelectric response. Synthesis of this nitride member of the broad family of perovskite structured materials with ABX_3 stoichiometry (for example, oxides, halides, and chalcogenides) suggests that other computationally predicted nitride perovskites with useful properties should be also possible to synthesize.

Materials with the perovskite crystal structure (Fig. 1A) are arguably the single most famous class of oxide compounds (*1*). Oxide perovskites, such as $Pb(Zr,Ti)O_3$ (PZT) and $(Ba,Sr)TiO_3$ (BST), with strong piezoelectric response have been extensively used for ceramic capacitors (*2*), microelectromechanical actuators (*3*), electrochemical cells (*4*), and many other applications (*5*, *6*) over the past century (*7*). In the past decade, research activity on halide (X = Cl, Br, or I) perovskites, such as $CH_3NH_3PbI_3$ and $CsPbI_3$, has skyrocketed because of their potential application as inexpensive and efficient optoelectronic devices (*8*). Giant optical anisotropy and nonlinear optics applications have recently attracted attention to chalcogenide (X = S or Se) perovskites, such as $BaTiS_3$ or $SrTiS_3$ (*9*). In contrast to oxides, chalcogenides, and halides, very few experimental reports of nitride perovskites exist in crystallographic databases or the literature (Fig. 1B). The few reported perovskites with high N content include powder $TaThN_3$ synthesized from oxide precursors (*10*) and powder $LaReN_3$ synthesized from azide precursors (*11*). Other known intermetallic materials, such as Mg_3SbN and Mn_3CuN, have an anti-perovskite structure and low N content (*12*). The relatively low number of reported nitride perovskites is surprising because pnictide (X = N or P) ABX_3 materials, including perovskites and others, are statistically more likely than the halide ABX_3 materials (Fig. 1B) because of a larger possible number of cation combinations that satisfy –9 collective anion valence versus the combinations for satisfying –3 collective anion valence (table S1). This leads us to the question of how to discover nitride perovskites and evaluate their potential properties.

Computationally driven experimental discovery is an effective approach to predict and synthesize new materials (*13*). In the field of nitrides, we recently synthesized ~10 ternary nitride materials out of ~200 computational predictions (*14*). Among nitride perovskites, $LnMN_3$ (Ln=La, Ce, Eu, Yb, M=W, and Re) materials were predicted by other groups to be thermodynamically stable (*15*, *16*), with lanthanum tungsten nitride ($LaWN_3$) having large 1750 meV/formula unit (f.u.) formation enthalpy. $LaWN_3$ was also predicted to have ferroelectric properties, with a large 61 $\mu C/cm^2$ spontaneous polarization and a small 110-meV barrier to polarization reversal (*17*). However, synthesis of $LaWN_3$ by using traditional bulk solid-state chemistry methods remains challenging (*18*), often leading to oxynitrides, such as $LaWO_{0.6}N_{2.4}$ (*19*). If pure nitride perovskites can be synthesized, a century of

[1]Materials Science Center, National Renewable Energy Laboratory, 15013 Denver West Parkway, Golden, CO 80401, USA. [2]Department of Metallurgical and Materials Engineering, Colorado School of Mines, 1500 Illinois Street, Golden, CO 80401, USA.
*Corresponding author. Email: andriy.zakutayev@nrel.gov (A.Z.); geoff.brennecka@mines.edu (G.L.B.)

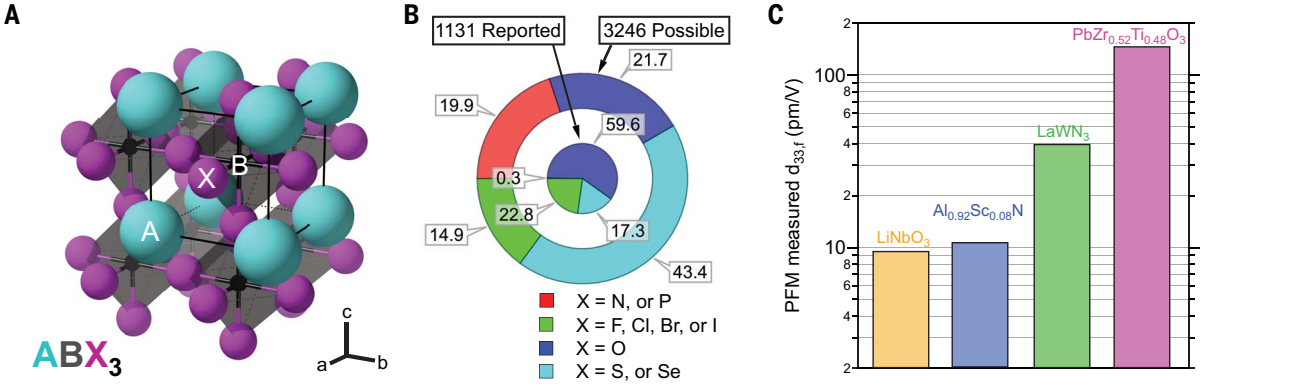

Fig. 1. Nitrides and other materials with the perovskite structure. (**A**) Cubic ABX_3 perovskite unit cell showing the larger A cation sites and smaller B cation sites in BX_6 octahedra. (**B**) Comparison of anion diversity in possible charge-balanced versus experimentally reported ABX_3 compounds, showing that pnictide perovskites are more likely but less reported than halide perovskites. (**C**) Comparison of piezoelectric materials measured in this work, demonstrating strong piezoelectric response of $LaWN_3$.

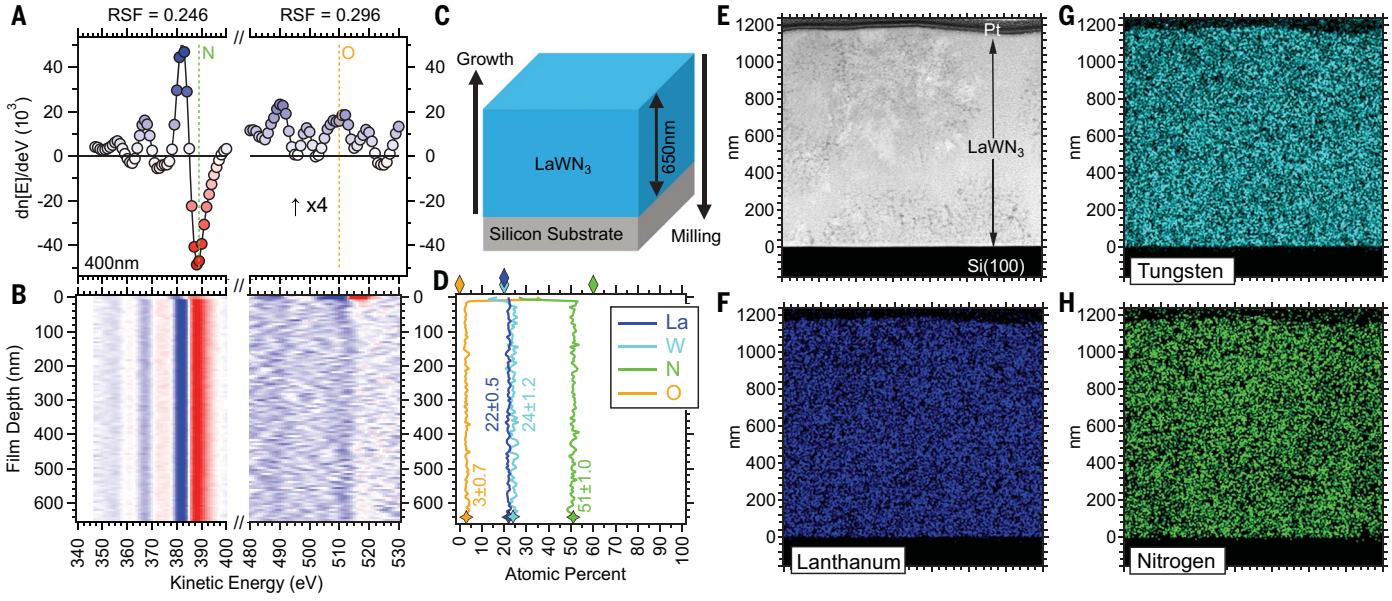

Fig. 2. Chemical composition of $LaWN_3$ thin films. (**A**) Differentiated AES results and (**B**) depth-resolved color intensity map for O and N, showing negligible O signal beyond a thin surface layer, where RSF is a relative sensitivity factor. (**C**) Depth profile and (**D**) resulting element concentration for all elements, with the average and ideal composition indicated with stars and diamonds at the bottom and top, respectively. (**E** to **H**) STEM and EDX images, showing a polycrystalline microstructure and chemical homogeneity of La, W, and N in $LaWN_3$ thin films.

experience in perovskite property engineering (*7*) could be combined with decades of advances in nitride semiconductor integration (*20*). This would likely have an enormous impact on both fundamental and applied research. We synthesized $LaWN_3$ nitride perovskite with polar symmetry and measured a piezoelectric response comparable with that of oxide perovskites and much greater than that of other known nitrides (Fig. 1C).

We used physical vapor deposition (combinatorial cosputtering) to synthesize crystalline $LaWN_3$ thin films on a heated substrate in ultrahigh vacuum to minimize O contamination, and with a N plasma source to maximize N incorporation (*21*). We detected no measurable O (below 3%) throughout the thickness of films beyond a thin nanometer-scale surface oxide layer (Fig. 2, A to D) by using Auger electron spectroscopy (AES), even after 72 hours of atmospheric exposure. These measurements were performed for a sample with the cation-stoichiometric composition (La/W = 1) as determined with x-ray fluorescence (XRF). However, our AES measurements indicate some N loss (51 atomic % instead of 60 atomic %), which can be written as $LaWN_{3-x}$ (x = 0.5) or $LaWN_{2.5}$. This N deficiency may result from either preferential N removal during AES depth profiling measurement (*21*) or the well-known tendency of the perovskite structure to accommodate large anion deficiency (*4*, *11*). Our scanning transmission electron microscopy (STEM) measurements with energy dispersive x-ray (EDX) analysis from the cross section of an identical film (Fig. 2, E to H) confirm a polycrystalline microstructure (150 to 200 nm grain size) and demonstrate chemical homogeneity on the nanometer scale. The corresponding x-ray diffraction (XRD) patterns of the cation-stoichiometric composition (La/W = 1) are consistent with the modeled phase-pure perovskite reference pattern, with W or WN and amorphous minor secondary phases at W- and La-rich compositions, respectively (fig. S1). We performed electrical and optical property measurements as a function of cation composition, which show 10^{-4} to 10^{4} ohm cm resistivity and 1.0 to 2.5 eV optical absorption onset with increasing La content (fig. S2). The upper bound of these measurements is the most representative of $LaWN_3$ because of the optoelectronically inert character of the amorphous lanthanum oxide second phase at La-rich compositions.

To determine the crystal structure of $LaWN_3$, we synthesized randomly oriented polycrystalline thin films by using rapid thermal annealing (RTA) of atomically dispersed amorphous La-W-N precursor films. These samples were sputter deposited on glass substrates and protected from oxidation with an AlN capping layer (*21*). The capped amorphous sample libraries were also free of O (fig. S3) and had a distinct color change close to the La/W = 1 composition (fig. S4), from black on the W-rich side to translucent yellow on the La-rich side. This yellow color is indicative of a <2.5 eV band gap. After the RTA, we observed a randomly oriented polycrystalline microstructure that was evident from uniform Debye-Scherrer rings (Fig. 3A). Our Rietveld refinement of the integrated XRD patterns (Fig. 3B) shows a majority perovskite phase along with a minority metallic W phase (<5% by volume) and possibly WN phase (<1% by volume) (table S2). For the perovskite crystal structure refinement, we chose candidate space groups (SGs) (table S3) calculated to be within ~100 meV/f.u. of the lowest-energy predicted R3c symmetry of $LaWN_3$ (*17*), as well as the higher-energy $I\bar{4}$ space group reported for the $LaWO_{0.6}N_{2.4}$ oxynitride perovskite (*19*). The structure refinement, performed for the unit cell lattice vectors and angles with all other variables held constant, resulted in low and statistically indistinguishable residuals for both the rhombohedral (R3c, SG 161) and tetragonal ($I\bar{4}$, SG 82) symmetries (fig. S5). We refined unit cell parameter (a) and angle (α) of the ground-state R3c perovskite structure to be a = 5.64 A, α = 60.33° in rhombohedral notation (*21*) and a = 5.67 A, c = 13.79 A in hexagonal notation, which is consistent with theoretical prediction for $LaWN_3$ (*17*). Our TEM-based selected area electron diffraction (SAED) results (Fig. 3, C to F) confirmed the perovskite structure that we determined using XRD and were similarly unable to resolve the nonpolar $I\bar{4}$ (SG 82) versus polar R3c (SG 161) structural distortions.

To distinguish between the two possible polar and nonpolar symmetries of $LaWN_3$ (*17*, *19*), we conducted piezoresponse force microscopy

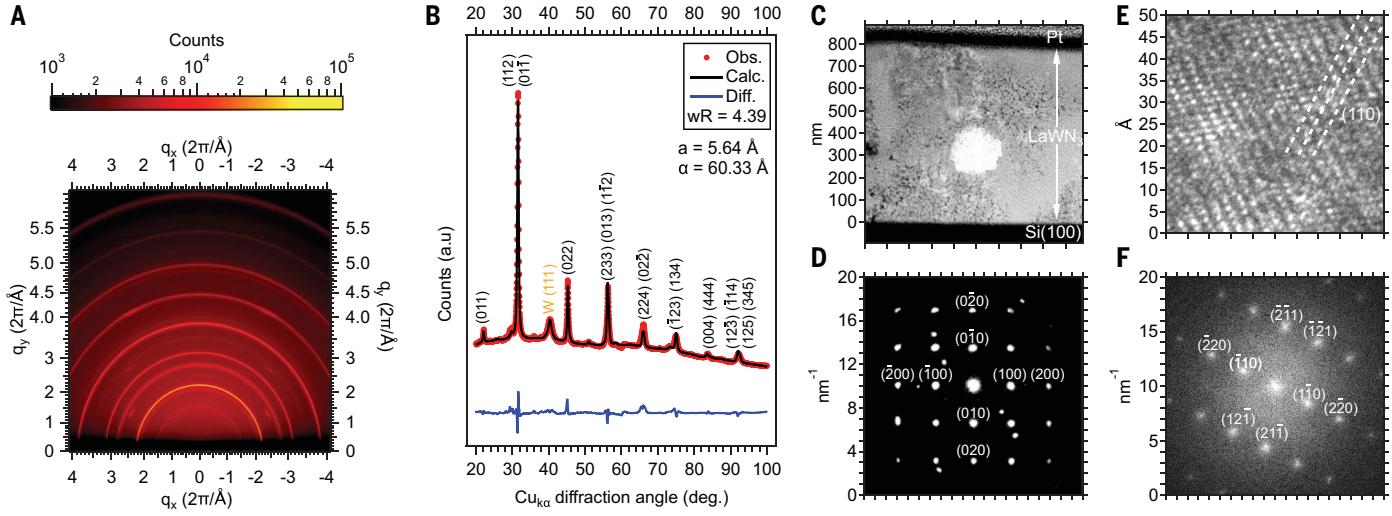

Fig. 3. Crystal structure of $LaWN_3$ thin films. (**A**) Two-dimensional XRD pattern, indicating randomly oriented polycrystalline microstructure. (**B**) Rietveld refinement of XRD data for $LaWN_3$ thin films with a predicted rhombohedral unit cell of R3c symmetry (space group 161) and body-centered cubic (bcc) tungsten (W) minority phase (<5% by volume). (**C**) STEM–HAADF (high angle annular dark field) image of an as-deposited crystalline film highlighting a single grain (white) and (**D**) SAED from this grain showing a pseudo-cubic perovskite [001]–type pattern. (**E**) High-resolution image of a single grain showing the pseudo-cubic (011) lattice spacing and (**F**) the associated fast Fourier transform indexed with a pseudo-cubic [113] type pattern.

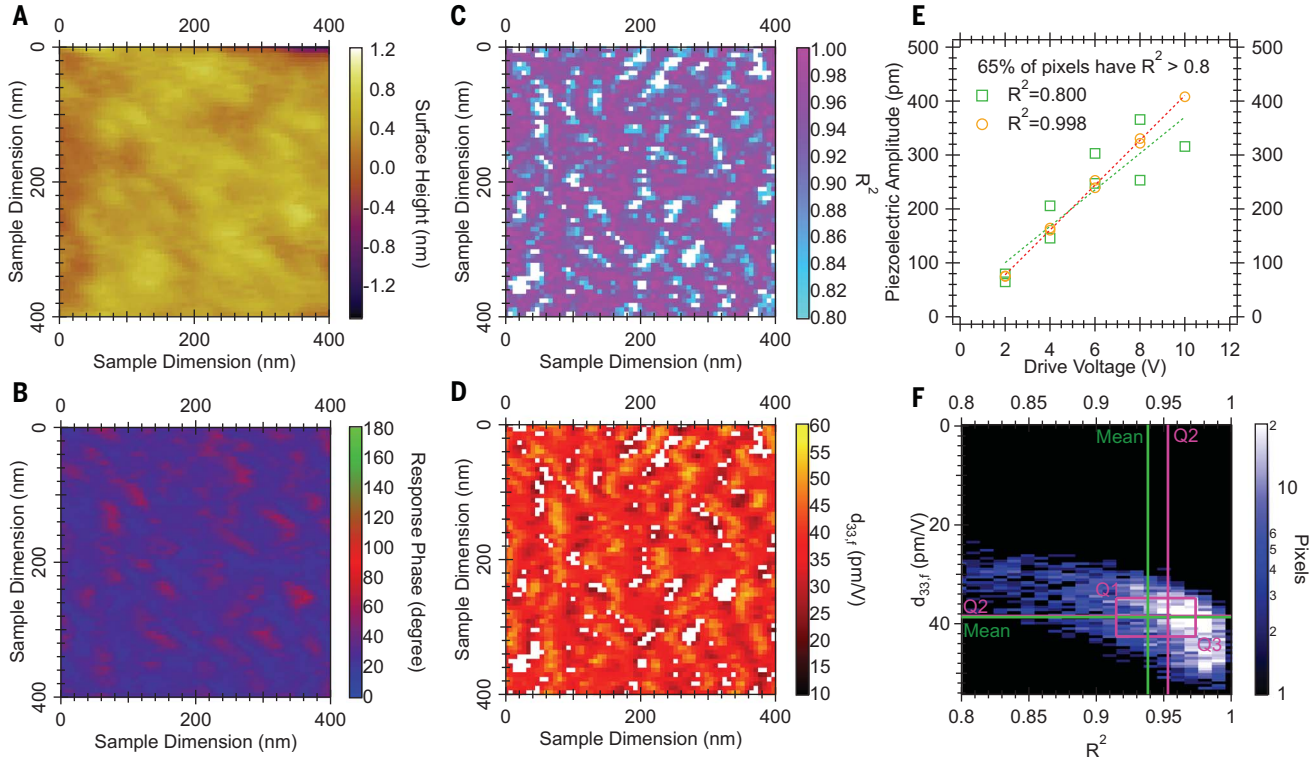

Fig. 4. Piezoelectric properties of $LaWN_3$ thin films. (**A**) Atomically smooth surface of a single $LaWN_3$ grain. (**B**) Phase, (**C**) linearity, and (**D**) slope of each of more than 4000 pixels with R^2 > 0.8 for piezoelectric amplitude versus drive voltage fits. (**E**) The best and worst fits included in this analysis resulting in (**F**) a three-dimensional histogram of these $d_{33,f}$ and R^2 values, indicating a mean (green) and median (magenta) value of the piezoelectric response. Analysis of $LiNbO_3$, PZT, and $(Al_{0.92}Sc_{0.08})N$ reference samples and details of the PFM measurements are provided in the supplementary materials (figs. S7 to S10).

(PFM) measurements (*21*) of the crystalline $LaWN_3$ film synthesized on the heated substrate (Fig. 1 and figs. S1 and S2). We used a <25-nm-radius tip to probe the electromechanical response of uncapped crystalline thin films that were insulating according to conductive atomic force microscopy (c-AFM) measurements (fig. S6). Our PFM results show qualitatively unambiguous piezoelectric response (Fig. 4, A to F), with 65% of more than 4000 pixels in a map (Fig. 4D) having coefficient of determination (R^2) > 0.8 fit of piezoelectric amplitude versus drive voltage (Fig. 4E). Our statistical analysis of these measurement results (Fig. 4F) in terms of mean and median

of all the pixels with $R^2 > 0.8$ indicate $d_{33,f}$ = 40 pm/V magnitude of effective piezoelectric strain coefficient. This $LaWN_3$ value (Fig. 1C) is four times larger than that of the $Al_{0.92}Sc_{0.08}N$ (~10 pm/V) and $LiNbO_3$ (~10 pm/V) reference samples (figs. S7 and S8) yet smaller than the highly engineered $PbZr_{0.52}Ti_{0.48}O_3$ reference sample (~150 pm/V) (fig. S9). Our PFM results clearly indicate a noncentrosymmetric unit cell, supporting the predicted R3c (SG 161) polar symmetry of $LaWN_3$ (*17*) and ruling out $I\bar{4}$ (SG 82) (*19*) as well as other centrosymmetric possibilities within ~100 meV/f.u. from the ground state (table S3). Although we are hesitant to claim quantitative values of piezoelectric coefficient from such PFM measurements (*22*), the results not only confirm polar symmetry of $LaWN_3$ but also indicate its strong piezoelectric response (Fig. 4, A to F).

Considering the computationally predicted ferroelectric character of $LaWN_3$ (17), we attempted to measure $LaWN_3$ polarization reversal (fig. S10, C and D). Our PFM measurements of the crystalline film (*21*) show that the phase of the piezoelectric response of a single 200-nm grain switches in the 0.25 to 0.50 MV/cm range of electric field. These values are similar to those of $PbZr_{0.52}Ti_{0.48}O_3$ that we measured under identical conditions (fig. S10), albeit with 150° instead of 180° phase change, indicating either incomplete switching or substantial charged-defect accumulation in the sample. Because of known challenges with such PFM ferroelectric measurements (*22*), we attempted domain writing across 10- by 10-μm area (fig. S10, E to H), but the results were inconclusive, suggesting the presence of defects at this larger scale. We also attempted macroscale electrical measurements for the samples with a narrow composition gradient and 100-μm-radius contacts (*21*), a process benchmarked by ferroelectric $Al_{1-x}Sc_xN$ thin films synthesized and characterized in our laboratory (*23*). We deposited these (111)-oriented perovskite films (fig. S11) on several conductive substrates (p^+ Si and Pt/Si) under many conditions—such as variations in total power, gas ratio, and film thickness—meant to simultaneously maximize crystallinity and minimize conductivity (fig. S11A). Despite multiple persistent attempts, we observed no definitive polarization-field (*P-E*) ferroelectric loops up to the measurement field of ~1 MV/cm, with the signal dominated by leakage current (fig. S11B). These microscale and macroscale electrical measurements are difficult because of a combination of residual minor impurities, such as metallic W or WN measured with XRD, and point defects, such as N deficiency suggested by AES. Synthesis of higher-quality $LaWN_3$ [theoretical band gap (E_g) = 1.8eV] or wider-gap $LaMoN_3$ (theoretical E_g = 2.7 eV) (*24*) may help decrease the leakage current and help determine whether these materials are indeed ferroelectric.

Nitride perovskites could substantially extend the range of possible applications of existing commercial nitride semiconductor devices. GaN, AlN, and related III-N alloys are well established for electronics in radio-frequency transistors, photonics in light emitting diodes, and telecommunication in film bulk acoustic resonators (*20*). Nitride perovskites may offer additional integration advantages compared with oxide perovskites on wurtzite nitrides. High-quality epitaxial layers of thermodynamically stable nitride perovskites (similar to oxide perovskites) would be easier to synthesize at high temperature than the recently reported metastable (Al,Sc)N wurtzite alloys with high (>30%) Sc content (*23*, *25*). Also, compared with oxide perovskites, nitride perovskites would be easier to integrate with GaN, similar to other nitride wurtzites. This is because there would be no competing N-O anion exchange reaction that results in interfacial layer formation known from growth of oxide perovskites on Si (*26*). Thus, epitaxial integration of nitride perovskites on nitride semiconductors may lead to entirely new types of devices for a broad range of applications (*20*), as highlighted by prospects of quantum computing and single-photon detectors in superconductor-semiconductor nitride heterostructures (*27*).

Our successful synthesis and characterization of $LaWN_3$ perovskite with polar symmetry should lead to more experimental measurements of its properties, as well as growth and characterization of many other theoretically predicted nitride perovskites. In addition to our measured strong piezoelectric response (40 pm/V) and published theoretically predicted ferroelectricity (*17*), there are multiple theoretical predictions of other interesting and useful $LaWN_3$ properties that await experimental confirmation, including spin textures (*28*) and p-type doping (*24*). The relatively narrow band gap of $LaWN_3$ (theoretical E_g = 1.8 eV) (*24*) compared with that of oxide perovskites (for example, E_g = 3.4 eV in $BaTiO_3$) could also offer an advantage in studying a controversial topic of solar energy conversion in perovskite materials with polar symmetry (*29*). Other nitride perovskites computationally predicted to have interesting properties are metallic $TbReN_3$ with very high anisotropy and large saturation magnetization (*16*) and $TaThN_3$ with topological insulating behavior (*30*). Nitride perovskites may also harbor other emergent properties or hidden states because of the mixed covalent and ionic character of the metal-nitrogen bonds that results from smaller electronegativity of N compared with O (*18*). Thus, our work on $LaWN_3$ opens the door to synthesis of other predicted nitride perovskites with exceptional electromechanical, magnetic, optoelectronic, thermoelectric, topological, and quantum properties.

REFERENCES AND NOTES

1. A. S. Bhalla, R. Guo, R. Roy, *Mater. Res. Innov.* **4**, 3–26 (2016).
2. D. Dimos, C. H. Mueller, *Annu. Rev. Mater. Sci.* **28**, 397–419 (1998).
3. P. Muralt, R. G. Polcawich, S. Trolier-McKinstry, *MRS Bull.* **34**, 658–664 (2009).
4. M. Papac, V. Stevanović, A. Zakutayev, R. O'Hayre, *Nat. Mater.* **20**, 301–313 (2021).
5. A. V. Boris *et al.*, *Science* **332**, 937–940 (2011).
6. X. Li *et al.*, *Science* **364**, 1079–1082 (2019).
7. V. M. Goldschmidt, *Naturwissenschaften* **14**, 477–485(1926).
8. M. M. Lee, J. Teuscher, T. Miyasaka, T. N. Murakami, H. J. Snaith, *Science* **338**, 643–647 (2012).
9. S. Niu *et al.*, *Nat. Photonics* **12**, 392–396 (2018).
10. N. E. Brese, F. J. DiSalvo, *J. Solid State Chem.* **120**, 378–380 (1995).
11. S. D. Kloß, M. L. Weidemann, J. P. Attfield, *Angew. Chem. Int. Ed.* **60**, 22260–22264 (2021).
12. R. Niewa, *Eur. J. Inorg. Chem.* **2019**, 3647–3660 (2019).
13. S. Curtarolo *et al.*, *Nat. Mater.* **12**, 191–201 (2013).
14. W. Sun *et al.*, *Nat. Mater.* **18**, 732–739 (2019).
15. R. Sarmiento-Pérez, T. F. Cerqueira, S. Körbel, S. Botti, M. A. Marques, *Chem. Mater.* **27**, 5957–5963 (2015).
16. J. A. Flores-Livas, R. Sarmiento-Pérez, S. Botti, S. Goedecker, M. A. Marques, *J. Phys. Mater.* **2**, 025003 (2019).
17. Y. W. Fang *et al.*, *Phys. Rev. B* **95**, 014111 (2017).
18. F. J. Disalvo, *Science* **247**, 649–655 (1990).
19. P. Bacher *et al.*, *J. Solid State Chem.* **77**, 67–71 (1988).
20. D. Jena *et al.*, *Jpn. J. Appl. Phys.* **58** (SC), SC0801 (2019).
21. Materials and methods are available as supplementary materials.
22. R. K. Vasudevan, N. Balke, P. Maksymovych, S. Jesse, S. V. Kalinin, *Appl. Phys. Rev.* **4**, 021302 (2017).
23. K. Yazawa, D. Drury, A. Zakutayev, G. L. Brennecka, *Appl. Phys. Lett.* **118**, 162903 (2021).
24. S. Singh, M. N. Tripathi, *J. Appl. Phys.* **124**, 065109 (2018).
25. S. Fichtner, N. Wolff, F. Lofink, L. Kienle, B. Wagner, *J. Appl. Phys.* **125**, 114103 (2019).
26. R. A. McKee, F. J. Walker, M. F. Chisholm, *Phys. Rev. Lett.* **81**, 3014–3017 (1998).
27. R. Yan *et al.*, *Nature* **555**, 183–189 (2018).
28. H. J. Zhao *et al.*, *Phys. Rev. B* **102**, 041203 (2020).
29. M.-M. Yang, D. J. Kim, M. Alexe, *Science* **360**, 904–907 (2018).
30. M. C. Jung, K.-W. Lee, W. E. Pickett, *Phys. Rev. B* **97**, 121104 (2018).

ACKNOWLEDGMENTS

Funding: This work was authored at the National Renewable Energy Laboratory, operated by Alliance for Sustainable Energy, for the US Department of Energy (DOE) under contract DE-AC36-08GO28308. Funding was provided by the Office of Science (SC), Office of Basic Energy Sciences (BES), Materials Chemistry Program, as a part of the Early Career Award "Kinetic Synthesis of Metastable Nitrides" (synthesis and characterization); as well as by the US National Science Foundation (NSF) Designing Materials to Revolutionize and Engineer our Future (DMREF) program (DMREF-1534503), and DARPA Tunable Ferroelectric Nitrides (TUFEN) program (DARPA-PA-19-04-03) (piezoelectric measurements). Use of the Stanford Synchrotron Radiation Lightsource, SLAC National Accelerator Laboratory, is supported by the US DOE, SC, BES under contract DE-AC02-76SF00515. The views expressed in the article do not necessarily represent the views of the DOE or the US government. **Author contributions:** K.R.T. synthesized the films, performed x-ray fluorescence and scattering measurements and piezoresponse force microscopy, and drafted the original version of the manuscript. C.L.P. performed AES measurements and commented on the manuscript. D.R.D. performed TEM measurements and commented on the manuscript. G.L.B. provided intellectual guidance and physical resources, assisted in data analysis, and edited the manuscript. A.Z. conceived the overall study; assisted in data analysis; provided intellectual guidance and physical resources; and edited, revised, and finalized the manuscript. **Competing interests:** The authors declare that they have no competing interests. **Data and materials availability:** All data are available in the main text or the supplementary materials.

SUPPLEMENTARY MATERIALS

science.org/doi/10.1126/science.abm3466
Materials and Methods
Supplemental Text
Figs. S1 to S11
Tables S1 to S3
References (*31*–*38*)
Data File S1

10 September 2021; accepted 30 October 2021
10.1126/science.abm3466

Synthesis of LaWN nitride perovskite with polar symmetry

Kevin R. TalleyCraig L. PerkinsDavid R. DiercksGeoff L. BrenneckaAndriy Zakutayev

Science, 374 (6574), • DOI: 10.1126/science.abm3466

Nitrides join the perovskite club

Perovskite structured materials have a variety of uses as photovoltaics, capacitors, and micromechanical actuators, along with other applications. Oxides, halides, and chalcogenides all have large numbers of perovskite structured materials. Examples of perovskite nitrides are conspicuously absent, but Talley *et al.* managed to synthesize one (see the Perspective by Hong). Lanthanum tungsten nitride in the perovskite structure turns out to be piezoelectric, which is ideal for a variety of applications. Perovskite structured nitrides are very attractive because they could easily integrate with the large number of nitride-based semiconducting devices already in use. —BG